Feedback-based Fault-tolerant and Health-adaptive Optimal Charging of Batteries

Sara Sattarzadeh¹, Shanthan K. Padisala¹, Ying Shi², Partha Pratim Mishra², Kandler Smith², Satadru Dey^{1,*}

Abstract

The key technology barriers that hinder the growth of Electric Vehicles (EVs) are long charging time, the shorter life-time of EV batteries, and battery safety. Specifically, EV charging protocols have significant effects on battery lifetime and safety. If not charged properly, the battery could end up with shorter life, and more importantly, improper charging can cause battery faults leading to catastrophic failures. To overcome these barriers, we propose a closed-loop feedback based approach, that enables real-time optimal fast charging protocol adaptation to battery health and possess active diagnostic capabilities in the sense that, during charging, it detects real-time faults and takes corrective action to mitigate such fault effects. We utilize battery electrical-thermal model, explicit battery capacity and power fade aging models, and thermal fault model to capture battery behavior. In conjunction with the models, we adopt linear quadratic optimal control techniques to realize the feedback-based control algorithm. Simulation studies are presented to illustrate the effectiveness of the proposed scheme.

Keywords:

Batteries, Optimal Fast Charging, Fault Tolerance, Battery Health.

^{*}Corresponding author: S. Dey

Email addresses: sfs6216@psu.edu (Sara Sattarzadeh), sfp5587@psu.edu (Shanthan K. Padisala), Ying.Shi@nrel.gov (Ying Shi), Partha.Mishra@nrel.gov (Partha Pratim Mishra), Kandler.Smith@nrel.gov (Kandler Smith), skd5685@psu.edu (Satadru Dey)

¹S. Sattarzadeh, S. K. Padisala, and S. Dey are with the Department of Mechanical Engineering, The Pennsylvania State University, University Park, PA 16802, USA.

²K. Smith is with National Renewable Energy Lab (NREL), Golden, CO 80401, USA. Y. Shi and P. P. Mishra were with NREL during the time of this work.

1. Introduction

1.1. Motivation and Challenges

A key barrier to greater electric vehicles adoption, which is crucial to decarbonize the transportation sector, is the longer charging time compared to the refueling time for internal combustion engine vehicles. Significant research efforts are ongoing to resolve this issue making EV charging a timely and relevant research area. However, there are some critical challenges in realizing such charging technologies. The first challenge is associated with battery degradation where the charging algorithms need to adapt to changing battery age. The second challenge is related to battery safety compromised by critical faults. Fast charging would result in high level of thermal and mechanical stresses, which not only induce nominal battery aging, but also significantly increase the probability of internal faults. Fast charging cause irreversible capacity loss due to the lithium deposition induced by high polarization. The deposited metal can solve into the electrolyte and can cause a separator puncture and consequently internal short circuit and thermal runaway. These internal faults can lead to accelerated, possibly catastrophic, battery failure [1]. Therefore, the charging control system must have active diagnostics/mitigation capabilities to detect these faults in their early stages reducing failure risks. Under this scenario, we propose a real-time feedbackbased optimal fast charging algorithm which adapts to battery health as the battery ages as well as ensures battery safety throughout its lifetime. In the next few subsections, we will discuss the state-of-the-art in literature followed by existing research gaps. Finally, we will discuss the main contributions of this work with respect to these research gaps.

1.2. Literature Review

In the past few years, several battery charging algorithms have been presented in literature. Broadly, these approaches can be divided into two categories. The first category is *model-free approaches* where the charging algorithm is designed based on heuristic methods. Some examples of such model-free approaches are: the widely used Constant Current Constant Voltage (CCCV) charging [2], multi-stage CCCV [3, 4, 5], fuzzy and neuro-fuzzy approach [6, 7], reinforcement learning approach [8], ant colony optimization approach [9], grey system theory based approach [10], and data-driven and

experimental validation approach [11]. Although these model-free approaches have the advantage of simple practical realization, the main drawback is unaccounted physical behavior of the batteries. Hence, these approaches may not be efficient or optimal from charging time or battery health point of view.

The second category, model-based approaches, overcomes the aforementioned limitation by explicitly considering battery physical models in the charging algorithm design. For example, [12] and [13] proposed linear quadratic control-based charging algorithms. In [14], an optimal charging profile is designed that minimizes charging time considering energy losses and temperature increase. Charging algorithms are presented in [1, 15, 16] based on control-oriented electrochemical models. Model predictive control based charging strategies are presented in [17], [18], [19], [20] and [21], [22], [23], [24], [25], [26]. Dynamic programming based charging algorithms are presented in [27], [28], [29], [30]. In [31], [32] and [33], pseudo-spectral methods based optimal charging strategies are presented.

In terms of fault detection, some techniques have been proposed in literature. For instance, in [34], a robust estimation algorithm is used to isolate thermal faults, and the loss of cooling system. Authors in [35] present a Lyapunov-based thermal parameter fault and heat generation fault diagnostic algorithm. In [36], authors propose a Kalman-filtering based thermal fault detection algorithm for large format batteries. The work in [37] proposes an uncertainty learning-based thermal fault detection algorithm for cylindrical cells under fast charging. The work in [38] utilizes an Lon Short Term Memory (LSTM)-Neural Network (NN) approach for detecting thermal faults. In [39], the time and location of battery pack faults are determined using big data and Shannon entropy analysis. However, the data-driven approaches [38, 39] have the disadvantage of requiring large amounts of data and may not be able to capture unforeseen anomalies. For details of the existing fault detection approaches, readers should refer to the comprehensive review papers [40, 41, 42]. Table 1 presents the summary of fault detection techniques.

1.3. Research Gaps

Most of the aforementioned model-based approaches suffer from one or more issues which will be discussed next. Many of these approaches ([12], [18], [14], [19], [43], [23], [44], [45]) do not consider battery health in their design. Some of the approaches account for battery health by posing constraints on battery internal states [13], [1], [17], [21], [27], [31], [33], [26], [22], [24]. Such internal state constraints can help maintain battery health to some

Table 1: Summary of fault detection techniques and their advantages and disadvantages

Technique	Advantages	Disadvantages
Robust estimation	Effective in isolating	May not detect other
algorithm [34]	thermal faults and loss	types of faults.
	of cooling system	
Lyapunov-based di-	Can diagnose thermal	May not be effective for
agnostic algorithm	parameter and heat gen-	other types of faults.
[35]	eration faults	
Kalman-filtering	Effective in detecting	Complexity may limit
based algorithm	thermal faults in large	real-time implementa-
[36]	format batteries	tion.
Uncertainty	Effective in detecting	Requires large amounts
learning-based	thermal faults during	of data.
algorithm [37]	fast charging of cylindri-	
	cal cells	
LSTM-NN ap-	Can detect thermal	Requires large amounts
proach [38]	faults using past data	of data and may not be
		effective for unforeseen
		anomalies.
Big data and Shan-	Can determine time and	Requires large amounts
non entropy analy-	location of faults	of data.
sis [39]		

extent. However, they may not able to capture comprehensive battery aging phenomena which do not affect such internal states under consideration.

The works [32] and [20] consider explicit battery aging dynamics. However, the approach in [32] does not account for deviation of actual aging from the a priori known aging model. The approach [20] is designed for online control purposes. However, it requires reference trajectories for battery State-of-Charge (SOC) and State-of-Health (SOH), which may not be available in practical situations. In [46] an electrochemical-thermal aged model is employed. However, the degradation consequences like resistance rise, capacity fade and temperature rise are not considered. The work [30] formulates the charging optimization problem based on the speed of capacity loss and energy loss of battery. However, this work utilizes the offline dynamic programming approach which may not be applied in real time as the battery

ages. Authors in [29, 15, 47, 48] consider the electrochemical-thermal aging model or Pseudo-two-Dimensional (P2D) model to capture the capacity fade due to Solid Electrolyte Interphase (SEI) growth and to obtain a fast charging protocol. However, the high computational cost of the model and algorithm limits the real-time application.

The works in [25, 49, 28] consider a reduced order P2D model or electrochemical model with SEI growth or lithium plating model and solve the fast charging problem. However, these works do not consider the temperature dynamics and temperature rise which is significantly affected by fast charging. In [26], an online model predictive control approach and P2D model is employed to solve the optimal charging problem. However, the authors do not consider the aging dynamics. In [50], an exponential current strategy and Single Particle (SP) model with hoop stress dynamics are considered in fast charging algorithm. However, no other degradation mechanisms are considered in this work. The work in [51] proposes a multi stage charging algorithm based on minimization of charging time and charging loss. Even so, the multi stage constant current strategies leads to more heat generation due to the switching of current in each stage [52]. Authors in [53] utilize the electrothermal aged model and Particle Swarm Optimization (PSO) algorithm to obtain a charging strategy which minimize the capacity loss. However, the power fade and resistance growth has not been considered in this work.

As mentioned in the last paragraph, although some of the aforementioned approaches have considered battery aging in terms of SEI growth or Lithium plating, it is difficult in practical applications to identify the model parameters of SEI or lithium plating models from the available measurements. It is important to note that different operating conditions like the driving pattern which reflects in current, SOC, and temperature are affecting the battery degradation. Motivated by that, in this work, we utilize an explicit aging model that captures the capacity fade and power fade as a function of those aforementioned conditions. Such explicit aging model is easier to identify from the available measurement data.

Finally, adapting to battery age is not enough. Fast charging would result in high level of thermal and mechanical stresses, which not only induce nominal battery aging, but also significantly increase the probability of internal faults that result in thermal runaway. These internal faults can lead to accelerated, possibly catastrophic, battery failure. Therefore, the charging control system must have active diagnostics/mitigation capabilities to detect these faults in their early stages reducing failure risks. None of the aforementioned

works possess such capabilities.

1.4. Literature Summary

Here, we summarize the literature review. Several model-based approaches for optimizing battery charging algorithms have been proposed. However, many of them do not consider battery health or only consider certain internal state constraints that may not fully capture comprehensive battery aging phenomena (e.g., [12, 18, 14, 19, 13, 1, 17]). Some approaches (e.g., [20, 30]) consider explicit battery aging dynamics, but they may require reference trajectories or have high computational costs that limit real-time application. Other approaches (e.g., [25, 51]) focus on reducing charging time or capacity fade but leave out other important dynamics. Finally, it is important to note that fast charging induces high levels of thermal and mechanical stresses, which can lead to internal faults that increase the probability of battery failure, and none of the aforementioned works have active fault diagnostics/mitigation capabilities.

1.5. Main Contribution

Based on the earlier review, we propose a safe and health-adaptive optimal fast charging algorithm that overcomes the aforementioned issues in existing approaches. Specifically, (i) the proposed approach considers battery electrical-thermal dynamics along with an explicit battery aging model that captures capacity fade and power fade; (ii) it does not require predetermined reference trajectories for battery SOC and SOH; (iii) it utilizes a closed-loop feedback based approach that enables real-time charging protocol adaptation to battery health, and (iv) most importantly, it possesses active diagnostic capabilities in the sense that it detects real-time faults during charging and takes corrective action to mitigate such fault effects. Some preliminary results of this work have been presented in the conference paper [54] where only the active fault-tolerant control aspect is discussed. However, the work [54] did not consider optimal charging problem nor did it consider the battery aging dynamics. This current paper extends the preliminary work [54] by (i) formulating and solving an optimal charging problem with consideration of battery capacity fade and power fade aging dynamics; and (ii) extending the fault-tolerant control scheme by employing the entropy effect as additional cooling mechanism to combat thermal anomalies.

1.6. Organization of the Paper

The rest of paper is organized as follows. In section 2 the battery electrical-thermal-aging model is discussed. Section 3 presents the proposed control algorithms for optimal fast charging including, the estimators and different control modes. In section 4 the results and discussion are presented and finally the paper is concluded in section 5.

2. Battery Model

In this section, we describe the battery modeling approach we have adopted for this work. We consider three aspects of the battery physical behavior in our model: (i) nominal electrical-thermal dynamics that represent the physical behavior of a new battery, (ii) battery aging reflected by capacity fade and power fade, and (iii) battery thermal faults that can potentially originate due to internal electrochemical failure, mechanical or thermal stress.

2.1. Nominal Battery Electrical-Thermal Model

In this work, we adopt an equivalent circuit model that captures battery electrical dynamics [55] (see Fig. 1). The equivalent circuit model consists of a voltage source that represents battery open circuit voltage (OCV), a series resistance (R) and a resistance-capacitance pair (R_1-C_1) . The mathematical representation of the equivalent circuit model is given as:

$$S\dot{O}C(t) = -\theta I(t),$$
 (1)

$$\dot{V}_c(t) = -\frac{V_c(t)}{R_1 C_1} + \frac{I(t)}{C_1},\tag{2}$$

$$V_t(t) = OCV(SOC) - V_c(t) - I(t)R,$$
(3)

where SOC is battery State-of-Charge, $\theta = 1/C_{bat}$ is inverse of battery capacity C_{bat} , V_c is the voltage across the capacitor C_1 , I is the applied battery current (I < 0 indicates charging and I > 0 indicates discharging), and V_t is the battery terminal voltage. To capture the battery thermal dynamics, we choose an average thermal model derived from energy balance principle [56].

$$mC_p \dot{T}(t) = -hA(T(t) - T_\infty(t)) + I(t)(OCV(SOC) - V_t(t) - T(t)\mu(SOC)), \quad (4)$$

where m is the battery mass in kg, C_p is the heat capacity in $Jkg^{-1}K^{-1}$, T is the average battery temperature in K, T_{∞} is the cooling temperature, h

is convective heat transfer coefficient in $(Wm^{-2}K^{-1})$, A is the area of heat transfer in m^2 and μ is the entropic heat coefficient as a function of SOC, as shown in Fig. 2 [57].

Note that there is always a trade-off between accuracy and complexity in battery models. For example, some Equivalent Circuit Models (ECMs) possess simple mathematical structure and reasonable computational requirements at the cost of potentially lesser accuracy. In comparison, some electrochemical models tend to be more accurate however at the cost of complex mathematical structure such as coupled nonlinear Partial Differential Equations. In this work, the proposed algorithms are designed for real-time control and diagnostic applications where simplified mathematical structure and lower computation aspects are required. Furthermore, under typical settings, characterization of electrochemical models tends to be more cumbersome than that of the ECMs. Due to these reasons, we have adopted a simplified ECM. The main limitations of using ECMs are the potential lack of accuracy. However, it is important to note that the use of feedback in the control and diagnostic algorithms in this framework will suppress the model uncertainties arising from inaccuracies to a reasonable extent. Specifically, the robustness properties of the sliding mode observer used in fault detection and estimation (discussed later in Section 3.1) will help address the uncertainties.

Remark 1. It is worth noting that the parameters R_0 , R_1 , and C_1 are typically affected by the operating conditions such as SOC, I, and T. However, characterization of such dependence typically requires cumbersome experimental efforts. Furthermore, explicitly incorporating such dependence within the model results in highly nonlinear model structure which in turn leads to two difficulties: (i) higher computation burden, and (ii) complex mathematical structure limiting the applicability of standard analysis and synthesis techniques. In order to avoid these difficulties, we have chosen to use constant values for these parameters – leading to simpler computation as well as use of standard analysis and design techniques. Furthermore, the model inaccuracies resulting from this choice of constant parameters are suppressed by the use of feedback in the control and diagnostic algorithms.

2.2. Battery Aging Model

Battery capacity and power fade affect the parameters (θ) and (R), respectively. Essentially, both θ and R increases as the battery ages over time.

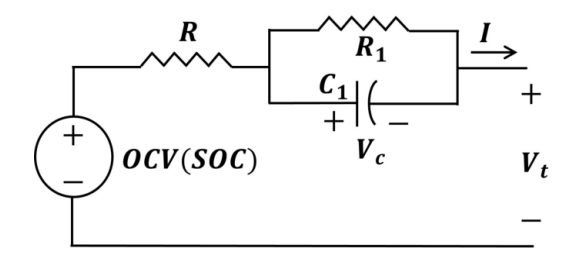


Figure 1: Battery electrical equivalent circuit.

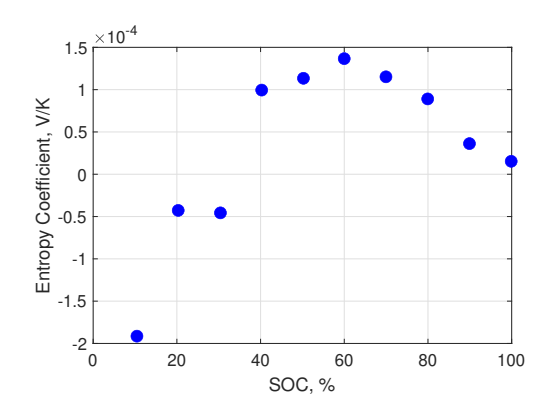


Figure 2: Entropy coefficient as a function of SOC [57].

Typically, such increase depends on battery SOC, average temperature T, current I, and depth of discharge (DOD). We consider the following aging models that capture the changes in θ and R:

$$\dot{\theta} = K_{\theta 1}\theta + K_{\theta 2}SOC + K_{\theta 3}T + K_{\theta 4}I + K_{\theta 5}DOD, \tag{5}$$

$$\dot{R} = K_{R1}R + K_{R2}SOC + K_{R3}T + K_{R4}I + K_{R5}DOD, \tag{6}$$

where DOD represents depth of discharge of the battery, $K_{\theta i}$ and K_{Ri} with i=1,...,5 are the coefficients of the aging model. The battery aging equations in (5) and (6) are an empirically fitted linear version of the degradation model developed by the National Renewable Energy Laboratory (NREL) [58, 59]. NREL's battery prognostic framework [58] has clearly established the dependency of battery degradation (capacity degradation and resistance growth) on important stress factors such as SOC, T, I, and DOD. However, these models are highly nonlinear in nature in order to capture changing dependencies throughout the life of the battery. To incorporate battery degradation into the fault tolerant control law, we considered a linear struc-

ture of the form $\dot{x} = \alpha x + \beta u$ for the battery life model. The coefficients of this model are identified through a linear least square regression (see Section 4.1), where the NREL developed, experimentally validated nonlinear battery degradation model [59] is used to generate "true" degradation and the linear model presented in (5) and (6) is used to obtain "predicted" value.

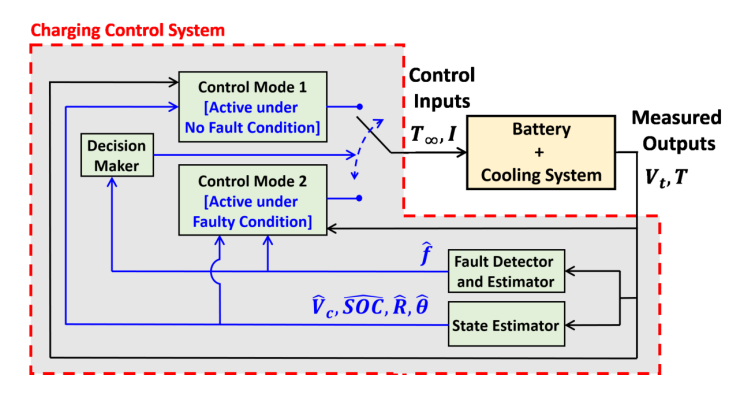


Figure 3: Charging control system schematic for safe and health-adaptive optimal fast charging. State estimator and fault detector and estimator generate estimates states and fault, respectively. Depending on the estimated fault, Control mode 1 is activated under no-fault condition while Control Mode 2 is activated under fault presence. Both control modes utilize real-time feedback of terminal voltage and temperature to generate control signals.

2.3. Battery Fault Model

As mentioned before, fast charging would result in high level of thermal and mechanical stresses which may lead to internal faults that result in thermal runaway. In this work, we model such internal faults as abnormal heat generation in the battery. Hence, under such faults, battery thermal model can be re-written as:

$$mC_{p}\frac{dT(t)}{dt} = -hA(T(t) - T_{\infty}(t)) + I(t)(OCV(SOC) - V_{t}(t) - T(t)\mu) + f(t), \quad (7)$$

where f represents the abnormal heat generation fault.

Remark 2. The term f represents the effect of physical faults that might lead to abnormal internal heat generation in the battery. Probable sources of such faults are [60, 36]: i) internal short circuit, ii) overcharging, iii) external mechanical or thermal abuse such as vibration and puncture.

Assumption 1. The functions OCV(.) and $\mu(.)$, and the parameters R_1 , C_1 , h, A, m, C_p , $K_{\theta i}$ and K_{Ri} with i = 1, ..., 5 are known a priori. These parameters can be found via offline data-driven identification techniques or online joint estimation algorithms. The temperature T and terminal voltage V_t are measured in real time. Finally, the value of DOD is known from the battery usage history.

3. Control System for Optimal Fast Charging

The schematic of the optimal fast charging algorithm is shown in Fig. 3. The charging control system consists of several subsystems whose functions are described as follows:

- State Estimator: This subsystem estimates the internal battery states SOC, V_c, R, θ online. As per our model formulation, the state SOC represents the amount of charge left in the battery, and the states R and θ represent battery SOH.
- Fault Detector and Estimator: This subsystem detects the occurrence of the fault f as well as estimates the magnitude or intensity of the fault online.
- Control Mode 1: This subsystem is active when there is no fault detected in the battery. It receives the feedback of measured terminal voltage (V_t) and temperature (T) and estimate of the states SOC, V_c, R , and θ , and in turn computes the charging current and cooling temperature based on a control law to be discussed later. The goal of this control mode is to ensure minimum time charging with consideration of battery health.
- Control Mode 2: This subsystem is active when there is a fault f in the battery. It also receives the feedback of measured V_t and T, estimates of the states SOC, V_c, R , and θ , and the estimate of the fault f. However, as opposed to minimum time charging, the goal of this control mode is to compute current and cooling temperature that minimizes the effect of fault f. Essentially, this mode is only active under safety emergency situations.
- Decision Maker: This subsystem decides which control mode to activate (Control Mode 1 or 2) based on the estimated fault feedback f. It

activates Control Mode 1 when no f is detected and activates Control Mode 2 when f is detected.

In the following, we will discuss the detail designs of the aforementioned subsystems.

Remark 3. Since battery state estimation has been widely explored in literature, we do not focus on that aspect of this work. We assume internal state estimates are available via some existing estimation techniques proposed in the literature (see, for example [61]). Note that aging processes evolve very slowly in time compared to charging dynamics. This phenomenon makes the battery system that exhibits multi time-scale behavior. There are a few works that explored multi time-scale aspects of battery charge and health-related parameters, such as [62, 63, 64]. Interested readers are suggested to refer to these works for details.

3.1. Fault Detector and Estimator

We follow a sliding mode observer based approach for designing the fault detector and estimator [65]. We chose the following observer structure.

$$mC_p \dot{\hat{T}} = -hA(\hat{T} - T_\infty) + I(OCV(S\hat{O}C) - V_t - T\mu) + L_T \operatorname{sgn}(T - \hat{T}), \quad (8)$$

$$\tau \dot{\hat{f}} = -\hat{f} + L_T \operatorname{sgn}(T - \hat{T}), \tag{9}$$

where \hat{f} is the estimate of the fault f, sgn(.) is the sign function, L_T is the observer gain to be designed and $\tau > 0$ is an user-defined parameter. Detailed design of the gain along with theoretical convergence analysis is shown in Appendix A. The filter given in (9) is implemented along with the detection observer (8), and used to estimate the fault magnitude online. The filter is essentially a first order low-pass filter that extracts the average value from the switching feedback signal $L_T \text{sgn}(T - \hat{T})$. Because of the properties of sliding mode, the average behavior of this switching feedback signal equal to the fault magnitude (see mathematical analysis in Appendix A). Hence, tracking this switching feedback signal allows us to reconstruct the fault online.

The fault detection logic is: a fault is detected when $\hat{f} > f_{th}$, otherwise no fault. In an ideal scenario with no modeling or measurement uncertainties,

the estimate $\hat{f} = 0$ when there is no fault and $\hat{f} \neq 0$ under a fault. However, due to the presence of modeling and/or measurement uncertainties, $\hat{f} \neq 0$ even when there is no fault. Hence, the threshold parameter f_{th} takes this into account and provides robustness to such uncertainties. The threshold f_{th} can be designed using the tuning according to the data collected under non-faulty conditions from Monte-Carlo simulations or experimental studies.

3.2. Decision Maker

The decision making logic is: activate Control Mode 1 when $\hat{f} \leq f_{th}$, and activate Control Mode 2 when $\hat{f} > f_{th}$.

3.3. Control Mode 1 - Fast Charging Mode

The objective of Control Mode 1 is to charge the battery within minimum time while considering the battery age. First, from (1)-(6), we formulate the battery state-space model by defining $x_1 = SOC - SOC_r, x_2 = V_c, x_3 = \theta$ and $x_4 = R$ where SOC_r is the constant target SOC to be reached after charging. The state-space model takes the following form:

$$\dot{x} = Ax + G(x)u + Dd,\tag{10}$$

with

$$A = \begin{bmatrix} 0 & 0 & 0 & 0 \\ 0 & -\frac{1}{R_1 C_1} & 0 & 0 \\ K_{\theta 2} & 0 & K_{\theta 1} & 0 \\ K_{R2} & 0 & 0 & K_{R1} \end{bmatrix}, \tag{11}$$

$$A = \begin{bmatrix} 0 & 0 & 0 & 0 \\ 0 & -\frac{1}{R_{1}C_{1}} & 0 & 0 \\ K_{\theta 2} & 0 & K_{\theta 1} & 0 \\ K_{R2} & 0 & 0 & K_{R1} \end{bmatrix},$$

$$G(x) = \begin{bmatrix} -x_{3} \\ \frac{1}{C_{1}} \\ K_{\theta 4} \\ K_{R4} \end{bmatrix}, D = \begin{bmatrix} 0 & 0 & 0 \\ 0 & 0 & 0 \\ K_{\theta 2} & K_{\theta 3} & K_{\theta 5} \\ K_{R2} & K_{R3} & K_{R5} \end{bmatrix},$$

$$(11)$$

where $x = [x_1, x_2, x_3, x_4]^T$ is the state vector, u = I is the control input, d = I $[SOC_r, T, DOD]^T$ is a known disturbance vector. Next, based on the statespace model (10), we pose the following optimization problem for minimumtime charging:

minimize
$$J = \alpha_1 x_1^2(t_f) + \alpha_2 x_3^2(t_f) + \alpha_3 x_4^2(t_f)$$

 $+ \alpha_4 \int_0^{t_f} 1 dt + \alpha_5 \int_0^{t_f} u^2 dt,$ (13)

subject to (10) where t_f is the free final time (that is, total charge time) and $\alpha_i > 0, i = 1, 2, ..., 5$ are the optimization weights to be selected by the user.

Remark 4. The first term in (13) represents the error between actual SOC and target SOC_r at final time t_f . The second and third terms $\alpha_2 x_3^2(t_f)$ and $\alpha_3 x_4^2(t_f)$ represents the value of inverse capacity θ and internal resistance R at final time $t = t_f$. Minimizing these two terms at final time essentially minimizes the power fade (i.e. increase in resistance) and capacity fade (i.e. decrease in capacity or equivalently, increase in θ). The fourth term minimizes the final time $t_f = \int_0^{t_f} 1 dt$ enabling fast charging. Finally, the fifth term represents a soft constraint on the total current during charging.

The objective function (13) can be written is the following compact form:

$$J = x^T(t_f)\overline{S}x(t_f) + \int_0^{t_f} (\alpha_4 + x^T Q_1 x + \alpha_5 u^2) dt, \qquad (14)$$

where the weight matrices \overline{S} and Q_1 are functions of the parameters $\alpha_1, \alpha_2, \alpha_3$ and α_4 . For further simplification, we re-write the model (10) as

$$\dot{x} = Ax + B_i u + Dd, (15)$$

where $B_i = G|_{\theta=\theta_i}$, $\theta_i \in [\overline{\theta}, \underline{\theta}]$ with $\overline{\theta}$ is the minimum possible capacity and $\underline{\theta}$ is the maximum possible capacity. Note that G_i is a constant vector evaluated at a given θ_i . This simplification leads to a linear system with known disturbances (15). To this end, the optimal control problem in hand is the following: Find the optimal control profile u^* during the time interval $t \in [0, t_f]$ that drives the system with known disturbances (15) along a state trajectory x^* such that the value of the cost function (14) is minimized, where the final time t_f and final state $x(t_f)$ are free parameters.

Following the calculus of variations, Lagrange multiplier approach and sweep method presented in [66], the solution to the aforementioned optimal control problem takes the following form:

$$-\dot{S} = SA + A^{T}S - SB_{i}\alpha_{5}^{-1}B_{i}^{T}S + Q_{1}, S(t_{f}) = \overline{S},$$
(16)

$$-\dot{M} = A^{T}M - SB_{i}\alpha_{5}^{-1}B_{i}^{T}M - SDd, M(t_{f}) = 0,$$
(17)

$$u = -K_1 x + K_2, K_1 = \alpha_5^{-1} B_i^T S, K_2 = \alpha_5^{-1} B_i^T M.$$
 (18)

The optimal control u is essentially an affine state feedback control with gains K_1 and K_2 . Note that the gains K_1 and K_2 depend on the trajectories S and M which in turn depend on B_i (equivalently on θ_i) and d (equivalently on DOD, T, SOC_r). Next, we compute the gains K_1 and K_2 offline by solving (16) and (17) for given ranges of $\theta_i \in [\overline{\theta}, \underline{\theta}], DOD \in [\overline{DOD}, \underline{DOD}], SOC_r \in [\overline{SOC_r}, \underline{SOC_r}]$ where $\overline{DOD}, \overline{T}, \overline{SOC_r}$ are the maximum values of the range and $\underline{DOD}, \underline{T}, \underline{SOC_r}$ are the minimum values of the range. Essentially, we compute the optimal control gains K_1 and K_2 for each possible values of θ, DOD, SOC_r, T . Next, these gains can be scheduled as a function of θ, DOD, SOC_r, T in real-time. Finally, the optimal control can be implemented in real-time as $u = -K_1(\theta, DOD, SOC_r, T)\hat{x} + K_2(\theta, DOD, SOC_r, T)$ where \hat{x} is the estimated state from the State Estimator and $K_1(.)$ and $K_2(.)$ are the gains scheduled as functions of θ, DOD, SOC_r, T .

3.4. Control Mode 2 - Fault-tolerant Mode

This control mode is active under the presence of a fault. The control objective is to mitigate the fault effect by minimizing the temperature rise. Note that safety is the primary concern in this mode, instead of fast charging. To achieve this objective, we take two measures. First, we treat cooling temperature T_{∞} as a control input and design a control algorithm that manipulates T_{∞} to minimize the temperature rise. Secondly, we utilize a discharging battery current I to further reduce the heat generation. This discharging battery current is chosen to achieve one of the two following objectives: (i) If the fault size is large, we discharge the battery to SOC = 0 condition. This is achieved to make sure that the battery is in lowest possible energy state under fault such that it emits lowest possible energy even if it explodes. (ii) If the fault size is small, we discharge the battery with small current to ensure that it stavs in the SOC region where the entropic coefficient $\mu(SOC)$ is positive. This will ensure that we get additional cooling effect from the entropic term. Algorithm 1 explains this thermal fault-tolerant scheme where f_{th} is the fault threshold that indicates a fault occurrence, f_{lim} is the fault threshold that distinguishes a large versus small fault, K_{f_1} and K_{f_2} are control gains, I_H and I_L are high and low discharge current under fault. The value I_H is manually tuned to balance the heat generation effect due to current and time taken to reach SOC = 0 state. The value I_L is tuned manually to balance the effect of heat due to current and the value of <u>SOC</u> is tuned to utilize the effect of cooling due to entropic term. The value f_{lim} is determined by the user considering the prior knowledge of cell thermal failure modes. Detailed design of the control gains are discussed in Appendix B.

Algorithm 1: Thermal Fault-tolerant Control Algorithm.

```
Input: Measured Temperature T, Estimated fault \hat{f}.

Output: Cooling Temperature T_{\infty}, Current I.

1 Read \hat{f};
2 if \hat{f} \leq f_{th} then

| DO NOTHING & GO TO Step 1;
else

| GO TO Step 3;

3 if \hat{f} > f_{lim} then

| Set T_{\infty} = K_{f_1}T + K_{f_2}\hat{f} and I = I_H;
else

| if 0 \leq SOC < \underline{SOC} then

| set T_{\infty} = K_{f_1}T + K_{f_2}\hat{f} and I = 0;
else

| set T_{\infty} = K_{f_1}T + K_{f_2}\hat{f} and I = I_L;
```

4. Results and Discussion

In this section we present the simulation studies of the proposed optimal charging control and fault-tolerant control algorithms to evaluate the performance of proposed schemes.

4.1. Battery Model and Parameterization

In these simulation studies the battery nominal parameters are taken from Table 1 of [67] which were originally studied and experimentally parameterized in [68]. The values are considered as follows: Q = 3921C, $R_1C_1 = 2631s$, $C_1 = 17327F$. Moreover, the thermal model parameters are taken from Table 5 of [69] and are as follows: $C_p = 1011JKg^{-1}K^{-1}$, $h = 21.04Wm^{-2}K^{-1}$, m = 0.039kg. For the battery life model, we use a semi-empirical degradation model developed by the National Renewable Energy Laboratory (NREL) as part of a battery life prognostics framework [58, 59]. In this framework,

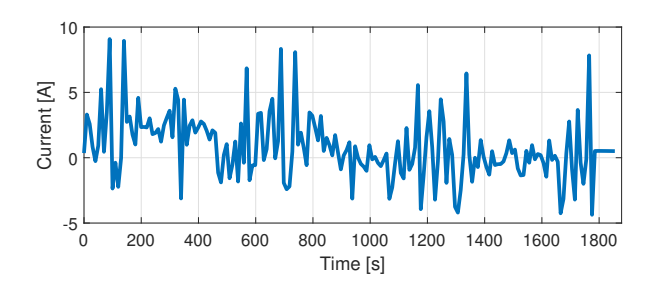


Figure 4: Discharge current profile in all simulation studies.

simple proxy models are used to capture the degradation trends in capacity and resistance based on several stress factors such as temperature, SOC, DOD, C-rate etc. The model itself is chemistry-specific as for each specific cell, there is need to test and re-parameterize the model to fit to each cell design's unique aging because aging rates (li-plating rate, SEI growth rate, etc) are sensitive to cell design and manufacturing quality (electrode material, binder, electrolyte, additives, coating procedures, wetting and drying procedures, etc.). Parameters for these models are identified using separate effects, accelerated aging test data [70]. We use a degradation model developed for LFP chemistry [71] as our "true" model and use linear least squares regression to identify the parameters $K_{\theta i}$ and K_{Ri} with $i = 1, \dots, 5$ in (5) and (6).

4.2. Results of optimal charging control

In this subsection, we demonstrate the performance of the proposed optimal charging control algorithm. We compare the performance of the proposed algorithm with the most common charging protocol, Constant-Current Constant-Voltage (CCCV). We charge the cell under different C-rates and compare the health degradation of the cell under each charging current profile. For the discharge part of the simulation, we have chosen the dynamic discharge current profile shown in Fig. 4. The applied optimal charging current profile during one year is illustrated in Fig. 5. The optimal charging profile is updated each month according to the health status of the cell given by (5) and (6). In order to investigate the performance of the optimal charging algorithm under model parameter uncertainties, we have injected uncertainties in the following parameters: (i) in R_1C_1 , which affects the A matrix in (15), and (ii) in θ which affects B_i in (15). The variations of control current trajectories are shown in Fig. 6. As it can be seen in in Fig. 6a, the

optimal charging profile is significantly robust with respect to uncertainties in R_1C_1 . On the other hand, the impact of uncertainties in B_i on control gains is relatively more and the changes in optimal charging profile can be seen in Fig. 6b.

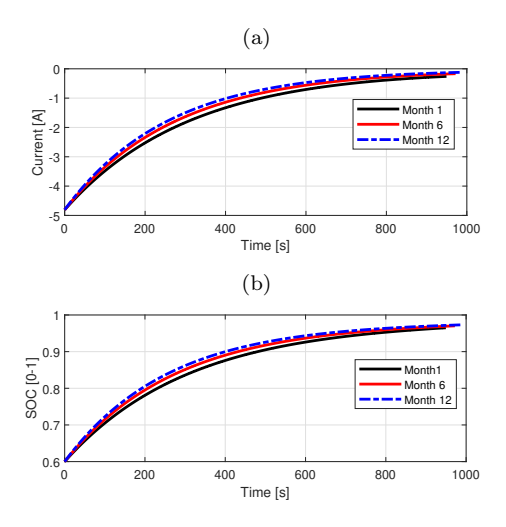


Figure 5: (a) Optimal charging current profile during one year; (b) SOC evolution under optimal current profile.

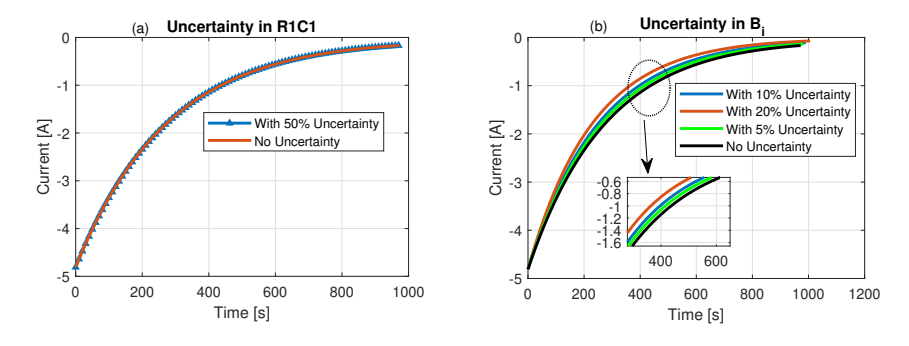


Figure 6: Optimal charging current profile in month six under parameter uncertainty.

In the optimal charging simulation, we consider the $SOC_r = 0.98$ and $SOC_0 = 0.6$. We consider three different CCCV charging profiles as 0.5C, 1C, 2C, in which C stands for C-rate. We compare the battery's performance under these three CCCV charging current profiles with the proposed optimal

charging current profile. The performance of the proposed optimal charging algorithm is evaluated in terms of charging time as well as capacity fade and resistance rise which are treated as the health indicators. As it is shown in the Fig. 7b, the capacity fade under the proposed optimal charging profile is less than the constant current case studies.

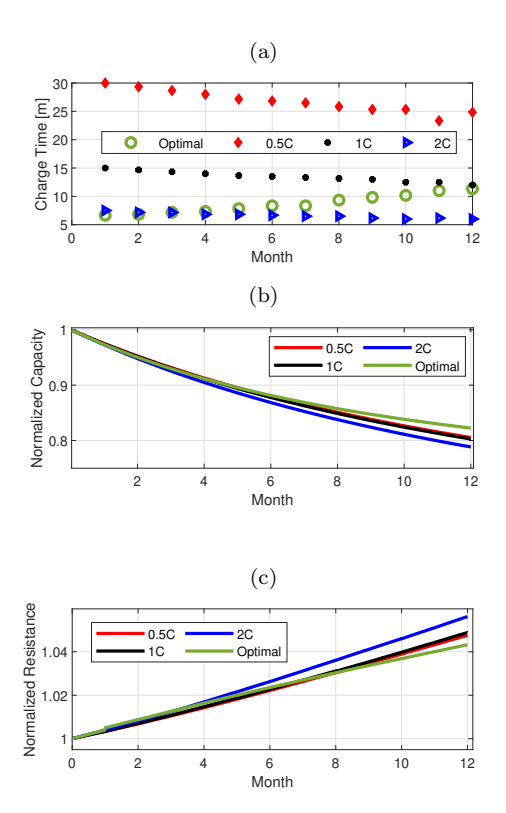


Figure 7: (a) Charge time comparison between different charging algorithms during one year; (b) Capacity fade during one year under different current profiles; (c) Resistance rise during one year under different current profiles.

In the case of optimal charging we obtain 17.73% capacity fade. However, in the cases that the cell was charged under constant current profile, we have 19.46%, 19.73%, and 21.16% capacity fade for 0.5C, 1C, and 2C current profiles, respectively. Moreover, the impedance rise under the optimal charging current profile is less than that under constant current charging profiles. There is 4.3% rise in the impedance under the optimal charging profile. However, there are 4.8%, 4.9%, and 5.6% impedance rise under 0.5C, 1C, and 2C current profiles, respectively. The charging time among all current

profiles are compared in Fig. 7a. We have compared the charging time under each current profile in the specific range of SOCs. The lower and upper SOC range for calculating and comparing the charging time are selected as SOC = 0.65 and SOC = 0.9, respectively. As it can be seen the charging time of the optimal current profile is close to the 2C (fast charging) profile at the beginning of the life and as the cell ages, the charging time lies between the charging time under 1C and 2C current profiles. However, the capacity fade and impedance rise in the optimal charging algorithm is considerably less than the constant fast charging current profile which enables more available peak power and longer driving range for the electric vehicle in long term. This is because of the proposed charging algorithm takes the time of charge as well as health of cell into consideration. As it can be seen from Fig. 7a to Fig. 7c, we have an optimal charging protocol which leads to less capacity fade and resistance rise which are the main concerns in fast charging algorithms. It should be mentioned that in these case studies we are representing the accelerated aging and the aggravated results by continued charge and discharge of cell, caused 20% capacity fade within one year. However, in reality the EV's customer using mainly the home charging, or the EV is parked in the parking lot most of the day, and they utilize the fast charging less often than it is simulated in this paper. Such charging routine makes the life-time of battery pack longer and slow the degradation behavior. In reality, the expected lifetime for EV's battery pack is 8 to 10 years.

4.3. Results of fault-tolerant Control

In this subsection, we present the simulation studies of the proposed fault-tolerant control algorithm. In these simulation studies we consider the $\beta_3 = 5$, $\beta_2 = 1$, $I_H = 1C$ and $I_L = 0.5C$, where C is the C-rate. Moreover, we consider the fault thresholds as follows: $f_{th} = 2$ Watt and $f_{lim} = 4$ Watt. The performance of the fault detector and estimator under no fault and faulty condition is demonstrated in Fig. 8. Here, the estimated states and faults are initialized with different conditions compared to the true values. Starting from these incorrect initial conditions, both state and fault estimates converge to the true values thereby proving the effectiveness of the algorithm. We perform the following case studies to evaluate the performance of the Algorithm 1 under different conditions:

• Case I: The fault magnitude is $\hat{f} = 5$ Watt which is greater than f_{lim} .

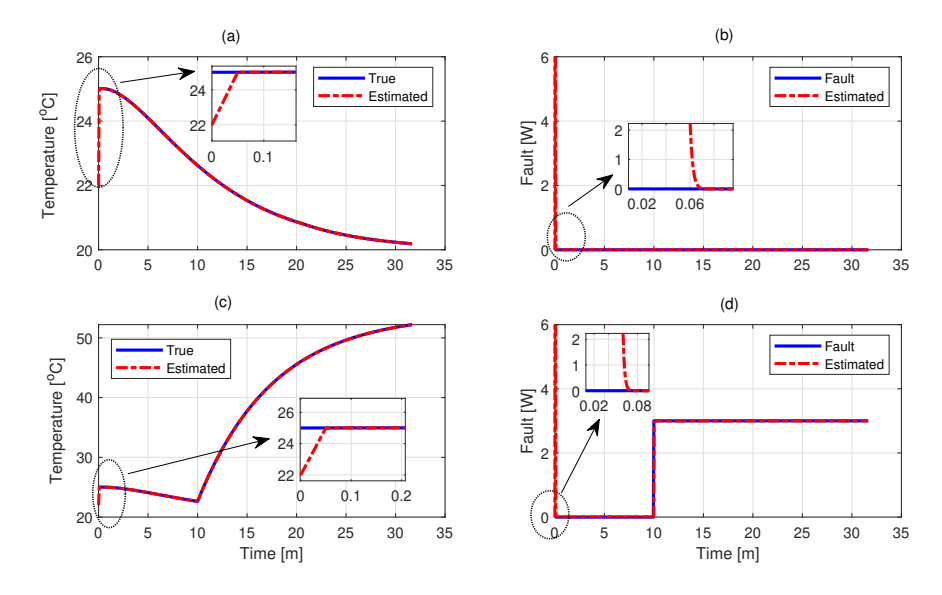


Figure 8: Fault detector and estimator performance. (a) Estimated temperature under no-fault; (b) Estimated fault under no-fault; (c) Estimated temperature under small fault; (d) Estimated fault.

• Case II: The fault magnitude is $\hat{f} = 3$ Watt, that is, $f_{th} < \hat{f} < f_{lim}$; and the SOC range is $0.4 \le SOC \le 1$.

The result of case studies are illustrated in Fig. 9 and Fig. 10. In Case I, we inject a large fault at t=10 min to evaluate the performance of the fault-tolerant control scheme. The fault estimation is shown in Fig. 9a. In Fig. 9b and Fig. 9e, the controlled current and and the controlled cooling temperature T_{∞} are shown. As it is shown, the fault-tolerant control algorithm is enabled at the time when the large fault is detected. Subsequently, the battery is being fully discharged by applying the I_H current to fully discharge the cell and avoid hazardous situation. In Fig. 9d, The performance of the fault-tolerant control algorithm is compared with the uncontrolled scenario when no control algorithm enables in case of fault occurrence. As it is demonstrated, the cell temperature remains in safe zone (below $50^{0}C$) under proposed fault-tolerant algorithm. The unsafe zone is depicted with red color.

In Case II, we inject the small fault, f = 3 watt at t = 10 min. In this scenario, the fault tolerant control algorithm is acting according to the SOC range. In this simulation study, we considered the $\underline{SOC} = 0.4$ according

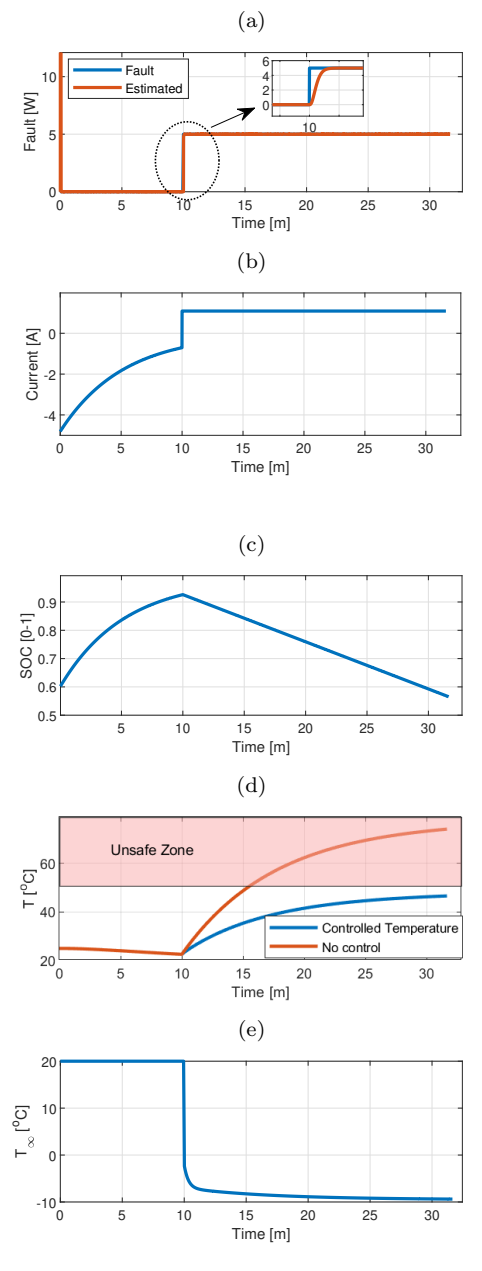


Figure 9: Case I results (a) The estimated fault; (b) Current profile; (c) Cell State of Charge; (d) Cell temperature; (e) Cooling temperature

to the entropy coefficient in Fig. 2. As it can be seen in the Fig. 10c, at

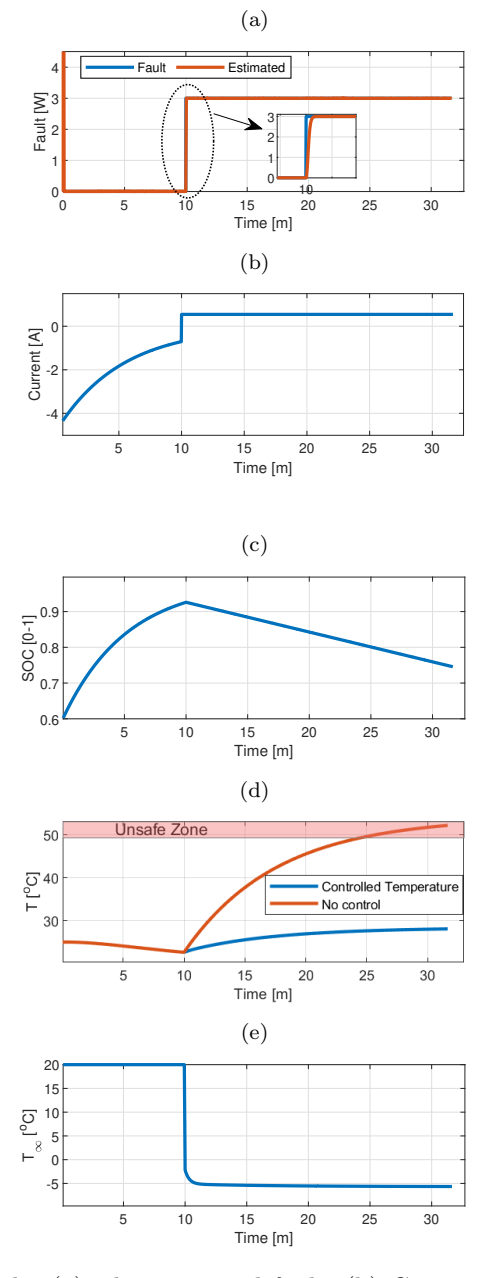


Figure 10: Case II results (a) The estimated fault; (b) Current profile; (c) Cell State of Charge; (d) Cell temperature; (e) Cooling temperature

the time of fault injection, the SOC range is higher than 0.4 and the fault-

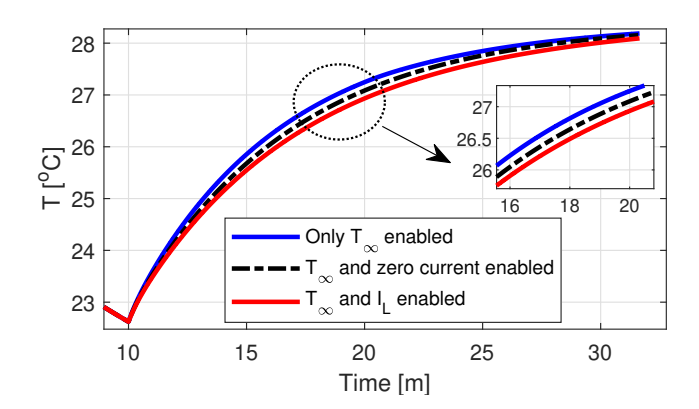


Figure 11: Controlled temperature with and without the effect of entropy.

tolerant control algorithm is enabled and applied the I_L to discharge the cell. By discharging the cell we utilize the effect of cooling due to the entropy term and consequently we observe less rise in temperature of cell.

The effect of entropic term can be seen in Fig. 11. To demonstrate the effect of entropic term, we consider three different scenarios after the fault is detected, as follows: (i) No change in current, that we only enable the controlled T_{∞} after the fault is detected and we keep charging the cell with the current as it was; (ii) Change the current to zero, that as the fault is detected, we change the current to zero as well as enabling the T_{∞} controller; (iii) Discharge the cell with I_L , that as the fault is detected we start discharging the cell with I_L as well as enabling the controlled T_{∞} . The result of each scenario is shown in Fig. 11. As it was expected, discharging the cell with I_L and utilizing the entropy effect help reducing the temperature in compare to the other two scenarios.

5. Conclusion

In this paper, we proposed a safe and health-adaptive optimal charging algorithm that considered battery electrical-thermal dynamics along with an explicit battery aging model that captured capacity fade and power fade. The proposed algorithm utilized a closed-loop feedback based approach that enabled real-time charging protocol adaptation to battery health, and most importantly posses active diagnostic capabilities in the sense that it detected real-time faults during charging and took corrective action to mitigate such

fault effects. The performance of proposed charging algorithm were evaluated and compared with the most common CCCV charging algorithm in terms of capacity fade, resistance rise, and charging time, showing improvements in less capacity fade and resistance rise with equivalently 1C to 2C charging speed. Moreover, we evaluated the performance of the proposed fault-tolerant control algorithm under different fault scenarios. As future extension of this work, we plan to compare the proposed algorithm other advance control methods like model predictive control to understand the detailed pros and cons of our approach. Furthermore, we also plan to run a detailed experimental campaign to verify the effectiveness of the proposed algorithm.

Acknowledgement

This work was primarily supported by National Science Foundation under Grants No. 1908560 and 2050315. The opinions, findings, and conclusions or recommendations expressed are those of the author(s) and do not necessarily reflect the views of the National Science Foundation. Funding for K. Smith and P. P. Mishra was provided by the DOE Office of Energy Efficiency and Renewable Energy's Vehicle Technologies Office under the guidance of the Advanced Battery Cell Research XCEL Program, technology manager Samuel Gillard. This manuscript was co-authored by the National Renewable Energy Laboratory operated by the Alliance for Sustainable Energy, LLC, for DOE under Contract No. DE-AC36-08GO28308. The U.S. Government retains and the publisher, by accepting the article for publication, acknowledges that the U.S. Government retains a non-exclusive, paid-up, irrevocable, worldwide license to publish or reproduce the published form of this manuscript, or allow others to do so, for U.S. Government purposes.

Appendix A. Theoretical Convergence Analysis of Fault Detector and Estimator

Here, we show the design of L_T by analyzing the error dynamics of the fault observer (8). Subtracting (8) from (7), and defining $\tilde{T} = T - \hat{T}$ as the state estimation error, we can write the error dynamics as:

$$mC_p\dot{\tilde{T}} = -hA\tilde{T} + f - L_T\operatorname{sgn}(\tilde{T}),$$
 (A.1)

We choose the Lyapunov function candidate $W_T = (1/2)mC_p\tilde{T}^2$ whose time derivative can be written as: $\dot{W}_T \leq |\tilde{T}|\{|f|-L_T\}$. With the choice of a sufficiently high gain such that $L_T > |f|, \forall t$, we have $\dot{W}_T < 0$ which in turn leads to the sliding motion defined by $\tilde{T}, \dot{\tilde{T}} \to 0$ [65]. Hence, under sliding motion, the error dynamics (A.1) can be written as $f = \varphi$ where φ is a average value of the switching signal $L_T \operatorname{sgn}(\tilde{T})$. For real-time implementation, the signal φ can be extracted by passing $L_T \operatorname{sgn}(\tilde{T})$ through a low-pass $L_T \operatorname{sgn}(\tilde{T})$ filter with unity steady-state gain. The equation (9) essentially represents such low-pass filter whose cut-off frequency depends on τ . The parameter τ can be tuned to meet the desired frequency response of the low-pass filter.

Appendix B. Theoretical Design of Control Mode 2

Here, we focus only on the thermal dynamics (7) and design the control gains K_{f_1} and K_{f_2} . Defining the state $\bar{X} = T$ and control input $U = T_{\infty}$, and considering $I = \{I_H, I_L\}$, (7) can be written as:

$$\dot{\bar{X}} = \bar{A}\bar{X} + \bar{g}(\bar{X}, I) + \bar{b}\bar{U} + \bar{c}\bar{f}, \tag{B.1}$$

where $\bar{A} = -(hA)/(mC_p)$, $\bar{b} = (hA)/(mC_p)$, $\bar{c} = 1/(mC_p)$, $\bar{g}(\bar{X}, I) = I(OCV(SOC) - V_t - \bar{X}\mu(SOC))$, and \bar{f} represents the fault. Linearizing (B.1) using Taylor's series expansion, we get the following linear approximation

$$\dot{X} = aX + bU + cf + d_2, \tag{B.2}$$

where X is the linearized temperature state, U is linearized cooling input, d_2 , and f contains the heating effect due to current and fault, and the system parameters $\{a, b, c\}$ are gain scheduled as functions of I and SOC. Based on (B.2), we pose the following optimization problem:

minimize
$$J = \beta_1 X(t_f)^2 + \frac{1}{2} \int_0^{t_f} (\beta_2 X^2 + \beta_3 U^2) dt,$$
 (B.3)

subject to (B.2) where t_f is the free final time and $\beta_i > 0, i = 1, 2, 3$ are the optimization weights to be selected by the user. In (B.3), the first term minimizes the final temperature, the first term inside the integral minimizes the temperature deviation within the whole time period, and the second term inside the integral provides a soft constraint on the cooling temperature T_{∞} . The problem structure is similar to (13) and can be posed as: Find the

optimal control profile U^* during the time interval $t \in [0, t_f]$ that drives the linear system with known disturbances (B.2) along a state trajectory X^* such that the value of the cost function (B.3) is minimized, where the final time t_f and final state $X(t_f)$ are free parameters. Following similar approach [66], the solution to the optimal control problem takes the following form:

$$-\dot{\mathbb{S}} = 2\mathbb{S}a + \beta_2 - \frac{\mathbb{S}^2b^2}{\beta_3},\tag{B.4}$$

$$-\dot{\mathbb{M}} = a\mathbb{M} - \frac{\mathbb{S}b^2}{\beta_3}\mathbb{M} + c\mathbb{S}f + \mathbb{S}d_2, \tag{B.5}$$

$$U = -\frac{b\mathbb{S}}{\beta_3}X + \frac{b}{\beta_3}\mathbb{M}, \mathbb{S}(t_f) = \beta_1, \mathbb{M}(t_f) = 0.$$
 (B.6)

For further simplification of (B.4) and (B.5), we consider the steady-state behavior \mathbb{S}_{∞} and \mathbb{M}_{∞} under the assumption $\dot{\mathbb{S}}, \dot{\mathbb{M}} \to 0, t \ll t_f$. Consequently, solving (B.4) and (B.5), with $\dot{\mathbb{S}}, \dot{\mathbb{M}} = 0$, results in:

$$\mathbb{S}_{\infty} = \frac{a\beta_3}{b^2} \left[1 - \sqrt{1 + \frac{\beta_2}{\beta_3}} \right], \mathbb{M}_{\infty} = \frac{\beta_3}{b^2} \left[1 - \sqrt{\frac{\beta_3}{\beta_3 + \beta_2}} \right] (cf + d_2), \quad (B.7)$$

Hence, comparing (B.7), (B.6), and Algorithm 1, the control gains are:

$$K_{f_1} = \frac{-a}{b} \left[1 - \sqrt{1 + \frac{\beta_2}{\beta_3}} \right],$$
 (B.8)

$$K_{f_2} = \frac{-1}{b} \left[1 - \sqrt{\frac{\beta_3}{\beta_3 + \beta_2}} \right] (cf + d_2),$$
 (B.9)

References

- [1] Z. Chu, X. Feng, L. Lu, J. Li, X. Han, M. Ouyang, Non-destructive fast charging algorithm of lithium-ion batteries based on the control-oriented electrochemical model, Applied Energy (2017).
- [2] D. Andrea, Battery management systems for large lithium-ion battery packs, Artech house, 2010.
- [3] S. S. Zhang, The effect of the charging protocol on the cycle life of a li-ion battery, Journal of power sources 161 (2006) 1385–1391.

- [4] Y.-H. Liu, C.-H. Hsieh, Y.-F. Luo, Search for an optimal five-step charging pattern for li-ion batteries using consecutive orthogonal arrays, IEEE Transactions on Energy Conversion 26 (2011) 654–661.
- [5] M. Abdel-Monem, K. Trad, N. Omar, O. Hegazy, P. Van den Bossche, J. Van Mierlo, Influence analysis of static and dynamic fast-charging current profiles on ageing performance of commercial lithium-ion batteries, Energy 120 (2017) 179–191.
- [6] Z. Ullah, B. Burford, S. Dillip, Fast intelligent battery charging: neural-fuzzy approach, IEEE Aerospace and Electronic Systems Magazine 11 (1996) 26–34.
- [7] H. Surmann, Genetic optimization of a fuzzy system for charging batteries, IEEE Transactions on Industrial Electronics 43 (1996) 541–548.
- [8] S. Park, A. Pozzi, M. Whitmeyer, H. Perez, A. Kandel, G. Kim, Y. Choi, W. T. Joe, D. M. Raimondo, S. Moura, A deep reinforcement learning framework for fast charging of li-ion batteries, IEEE Transactions on Transportation Electrification 8 (2022) 2770–2784. doi:10.1109/TTE. 2022.3140316.
- [9] Y.-H. Liu, J.-H. Teng, Y.-C. Lin, Search for an optimal rapid charging pattern for lithium-ion batteries using ant colony system algorithm, IEEE Transactions on Industrial Electronics 52 (2005) 1328–1336.
- [10] L.-R. Chen, R. C. Hsu, C.-S. Liu, A design of a grey-predicted li-ion battery charge system, IEEE Transactions on Industrial Electronics 55 (2008) 3692–3701.
- [11] F. B. Spingler, W. Wittmann, J. Sturm, B. Rieger, A. Jossen, Optimum fast charging of lithium-ion pouch cells based on local volume expansion criteria, Journal of Power Sources 393 (2018) 152–160.
- [12] Y. Parvini, A. Vahidi, Maximizing charging efficiency of lithium-ion and lead-acid batteries using optimal control theory, in: American Control Conference (ACC), 2015, IEEE, 2015, pp. 317–322.
- [13] H. Fang, Y. Wang, J. Chen, Health-aware and user-involved battery charging management for electric vehicles: Linear quadratic strategies, IEEE Transactions on Control Systems Technology 25 (2017) 911–923.

- [14] A. Abdollahi, X. Han, G. Avvari, N. Raghunathan, B. Balasingam, K. Pattipati, Y. Bar-Shalom, Optimal battery charging, part i: Minimizing time-to-charge, energy loss, and temperature rise for ocv-resistance battery model, Journal of Power Sources 303 (2016) 388–398.
- [15] C. Liu, Y. Gao, L. Liu, Toward safe and rapid battery charging: Design optimal fast charging strategies thorough a physics-based model considering lithium plating, International Journal of Energy Research 45 (2021) 2303–2320.
- [16] Y. Yin, Y. Bi, Y. Hu, S.-Y. Choe, Optimal fast charging method for a large-format lithium-ion battery based on nonlinear model predictive control and reduced order electrochemical model, Journal of The Electrochemical Society 167 (2021) 160559.
- [17] J. Liu, G. Li, H. K. Fathy, An extended differential flatness approach for the health-conscious nonlinear model predictive control of lithiumion batteries, IEEE Transactions on Control Systems Technology 25 (2017) 1882–1889.
- [18] M. Torchio, N. A. Wolff, D. M. Raimondo, L. Magni, U. Krewer, R. B. Gopaluni, J. A. Paulson, R. D. Braatz, Real-time model predictive control for the optimal charging of a lithium-ion battery, in: American Control Conference (ACC), 2015, IEEE, 2015, pp. 4536–4541.
- [19] C. Zou, X. Hu, Z. Wei, X. Tang, Electrothermal dynamics-conscious lithium-ion battery cell-level charging management via state-monitored predictive control, Energy 141 (2017) 250–259.
- [20] C. Zou, Modelling, state estimation & optimal charging control for a lithium-ion battery (2016).
- [21] R. Klein, N. A. Chaturvedi, J. Christensen, J. Ahmed, R. Findeisen, A. Kojic, Optimal charging strategies in lithium-ion battery, in: American Control Conference (ACC), 2011, IEEE, 2011, pp. 382–387.
- [22] C. Zou, X. Hu, Z. Wei, T. Wik, B. Egardt, Electrochemical estimation and control for lithium-ion battery health-aware fast charging, IEEE Transactions on Industrial Electronics 65 (2017) 6635–6645.

- [23] A. Pozzi, M. Torchio, R. D. Braatz, D. M. Raimondo, Optimal charging of an electric vehicle battery pack: A real-time sensitivity-based model predictive control approach, Journal of Power Sources 461 (2020) 228133.
- [24] N. Tian, H. Fang, Y. Wang, Real-time optimal lithium-ion battery charging based on explicit model predictive control, IEEE Transactions on Industrial Informatics (2020).
- [25] Y. Yin, Y. Bi, Y. Hu, S.-Y. Choe, Optimal fast charging method for a large-format lithium-ion battery based on nonlinear model predictive control and reduced order electrochemical model, Journal of the Electrochemical Society (2020).
- [26] S. Kolluri, S. V. Aduru, M. Pathak, R. D. Braatz, V. R. Subramanian, Real-time nonlinear model predictive control (nmpc) strategies using physics-based models for advanced lithium-ion battery management system (bms), Journal of The Electrochemical Society 167 (2020) 063505.
- [27] R. Methekar, V. Ramadesigan, R. D. Braatz, V. R. Subramanian, Optimum charging profile for lithium-ion batteries to maximize energy storage and utilization, ECS Transactions 25 (2010) 139–146.
- [28] X. Lin, X. Hao, Z. Liu, W. Jia, Health conscious fast charging of li-ion batteries via a single particle model with aging mechanisms, Journal of Power Sources 400 (2018) 305–316.
- [29] M. Xu, R. Wang, P. Zhao, X. Wang, Fast charging optimization for lithium-ion batteries based on dynamic programming algorithm and electrochemical-thermal-capacity fade coupled model, Journal of Power Sources 438 (2019) 227015.
- [30] Y. Lei, C. Zhang, Y. Gao, T. Li, Charging optimization of lithium-ion batteries based on capacity degradation speed and energy loss, Energy Procedia 152 (2018) 544–549.
- [31] X. Hu, S. Li, H. Peng, F. Sun, Charging time and loss optimization for linms and lifepo 4 batteries based on equivalent circuit models, Journal of Power Sources 239 (2013) 449–457.

- [32] H. Perez, X. Hu, S. Dey, S. Moura, Optimal charging of li-ion batteries with coupled electro-thermal-aging dynamics, IEEE Transactions on Vehicular Technology (2017).
- [33] H. Perez, S. Dey, X. Hu, S. Moura, Optimal charging of li-ion batteries via a single particle model with electrolyte and thermal dynamics, Journal of The Electrochemical Society 164 (2017) A1679—A1687.
- [34] J. Marcicki, S. Onori, G. Rizzoni, Nonlinear fault detection and isolation for a lithium-ion battery management system, in: ASME 2010 Dynamic Systems and Control Conference, American Society of Mechanical Engineers Digital Collection, 2010, pp. 607–614.
- [35] J. Wei, G. Dong, Z. Chen, Lyapunov-based thermal fault diagnosis of cylindrical lithium-ion batteries, IEEE Transactions on Industrial Electronics (2019).
- [36] S. Sattarzadeh, T. Roy, S. Dey, Thermal fault detection and localization framework for large format batteries, Journal of Power Sources 512 (2021) 230400.
- [37] R. Firoozi, S. Sattarzadeh, S. Dey, Cylindrical battery fault detection under extreme fast charging: A physics-based learning approach, IEEE Transactions on Energy Conversion 37 (2022) 1241–1250. doi:10.1109/TEC.2021.3112950.
- [38] O. Ojo, H. Lang, Y. Kim, X. Hu, B. Mu, X. Lin, A neural network-based method for thermal fault detection in lithium-ion batteries, IEEE Transactions on Industrial Electronics (2020).
- [39] J. Hong, Z. Wang, P. Liu, Big-data-based thermal runaway prognosis of battery systems for electric vehicles, Energies 10 (2017) 919.
- [40] R. Xiong, W. Sun, Q. Yu, F. Sun, Research progress, challenges and prospects of fault diagnosis on battery system of electric vehicles, Applied Energy 279 (2020) 115855.
- [41] X. Hu, K. Zhang, K. Liu, X. Lin, S. Dey, S. Onori, Advanced Fault Diagnosis for Lithium-Ion Battery Systems: A Review of Fault Mechanisms, Fault Features, and Diagnosis Procedures, IEEE Industrial Electronics Magazine 14 (2020) 65–91.

- [42] M.-K. Tran, M. Fowler, A review of lithium-ion battery fault diagnostic algorithms: Current progress and future challenges, Algorithms 13 (2020) 62.
- [43] J. Sun, Q. Ma, R. Liu, T. Wang, C. Tang, A novel multiobjective charging optimization method of power lithium-ion batteries based on charging time and temperature rise, International Journal of Energy Research 43 (2019) 7672–7681.
- [44] Q. Ouyang, J. Chen, J. Zheng, H. Fang, Optimal multiobjective charging for lithium-ion battery packs: A hierarchical control approach, IEEE Transactions on Industrial Informatics 14 (2018) 4243–4253.
- [45] Q. Ouyang, G. Xu, H. Fang, Z. Wang, Fast charging control for battery packs with combined optimization of charger and equalizers, IEEE Transactions on Industrial Electronics (2020).
- [46] K. Liu, C. Zou, K. Li, T. Wik, Charging pattern optimization for lithium-ion batteries with an electrothermal-aging model, IEEE Transactions on Industrial Informatics 14 (2018) 5463–5474.
- [47] F. Lam, A. Allam, W. T. Joe, Y. Choi, S. Onori, Offline multiobjective optimization for fast charging and reduced degradation in lithium-ion battery cells using electrochemical dynamics, IEEE Control Systems Letters (2020).
- [48] A. Pozzi, M. Torchio, D. M. Raimondo, Film growth minimization in a li-ion cell: a pseudo two dimensional model-based optimal charging approach, in: 2018 European Control Conference (ECC), IEEE, 2018, pp. 1753–1758.
- [49] M. Song, S.-Y. Choe, Fast and safe charging method suppressing side reaction and lithium deposition reaction in lithium ion battery, Journal of Power Sources 436 (2019) 226835.
- [50] B. Lu, Y. Zhao, Y. Song, J. Zhang, Stress-limited fast charging methods with time-varying current in lithium-ion batteries, Electrochimica Acta 288 (2018) 144–152.
- [51] G.-J. Chen, Y.-H. Liu, S.-C. Wang, Y.-F. Luo, Z.-Z. Yang, Searching for the optimal current pattern based on grey wolf optimizer and equivalent

- circuit model of li-ion batteries, Journal of Energy Storage 33 (2021) 101933.
- [52] W. Xie, X. Liu, R. He, Y. Li, X. Gao, X. Li, Z. Peng, S. Feng, X. Feng, S. Yang, Challenges and opportunities toward fast-charging of lithiumion batteries, Journal of Energy Storage 32 (2020) 101837.
- [53] X. Hu, Y. Zheng, X. Lin, Y. Xie, Optimal multistage charging of nca/graphite lithium-ion batteries based on electro-thermal-aging dynamics, IEEE Transactions on Transportation Electrification (2020).
- [54] S. Dey, Y. Shi, K. Smith, M. Khanra, Safer batteries via active fault tolerant control, in: 2019 American Control Conference (ACC), IEEE, 2019, pp. 1561–1566.
- [55] G. L. Plett, Battery management systems, Volume I: Battery modeling, Artech House, 2015.
- [56] D. Bernardi, E. Pawlikowski, J. Newman, A general energy balance for battery systems, Journal of the electrochemical society 132 (1985) 5–12.
- [57] Entropy Coefficient and Thermal Time Constant Estimation From Dynamic Thermal Cycling of a Cylindrical LiFePO4 Battery Cell, volume 2 of *Dynamic Systems and Control Conference*, 2014.
- [58] National Renewable Energy Laboratory, BLAST: Battery lifetime analysis and simulation tool suite, Available at www.nrel.gov/transportation/blast.html (Accessed 12/03/2018), ????
- [59] S. Santhanagopalan, K. Smith, J. Naubauer, G.-H. Kim, M. Keyser, A. Pesaran, Design and analysis of large Lithium-ion battery systems, Artech House, Boston USA, 2015.
- [60] D. H. Doughty, E. P. Roth, A general discussion of li ion battery safety, The Electrochemical Society Interface 21 (2012) 37–44.
- [61] M. A. Xavier, J. T. Hughes, A model-based approach for correcting state of charge drift in hybrid electric vehicles, in: 2020 IEEE Conference on Control Technology and Applications (CCTA), IEEE, 2020, pp. 673– 678.

- [62] C. Yang, X. Wang, Q. Fang, H. Dai, Y. Cao, X. Wei, An online soc and capacity estimation method for aged lithium-ion battery pack considering cell inconsistency, Journal of Energy Storage 29 (2020) 101250.
- [63] Y. Hua, A. Cordoba-Arenas, N. Warner, G. Rizzoni, A multi time-scale state-of-charge and state-of-health estimation framework using nonlinear predictive filter for lithium-ion battery pack with passive balance control, Journal of Power Sources 280 (2015) 293–312.
- [64] C. Zou, C. Manzie, D. Nešić, A. G. Kallapur, Multi-time-scale observer design for state-of-charge and state-of-health of a lithium-ion battery, Journal of Power Sources 335 (2016) 121–130.
- [65] V. Utkin, J. Guldner, J. Shi, Sliding mode control in electro-mechanical systems, volume 34, CRC press, 2009.
- [66] F. L. Lewis, D. Vrabie, V. L. Syrmos, Optimal control, John Wiley & Sons, 2012.
- [67] M. J. Rothenberger, D. J. Docimo, M. Ghanaatpishe, H. K. Fathy, Genetic optimization and experimental validation of a test cycle that maximizes parameter identifiability for a li-ion equivalent-circuit battery model, Journal of Energy Storage 4 (2015) 156–166.
- [68] D. Docimo, M. Ghanaatpishe, H. K. Fathy, Development and experimental parameterization of a physics-based second-order lithium-ion battery model, in: Dynamic Systems and Control Conference, volume 46186, American Society of Mechanical Engineers, 2014, p. V001T19A003.
- [69] P. Keil, K. Rumpf, A. Jossen, Thermal impedance spectroscopy for li-ion batteries with an ir temperature sensor system, in: 2013 World Electric Vehicle Symposium and Exhibition (EVS27), IEEE, 2013, pp. 1–11.
- [70] K. Smith, A. Saxon, M. Keyser, B. Lundstrom, Ziwei Cao, A. Roc, Life prediction model for grid-connected li-ion battery energy storage system, in: 2017 American Control Conference (ACC), 2017, pp. 4062–4068.

[71] P. P. Mishra, A. Latif, M. Emmanuel, Y. Shi, K. McKenna, K. Smith, A. Nagarajan, Analysis of degradation in residential battery energy storage systems for rate-based use-cases, Applied Energy 264 (2020) 114632. URL: https://www.sciencedirect.com/science/article/pii/S0306261920301446. doi:https://doi.org/10.1016/j.apenergy.2020.114632.